p-ISSN 2089 – 0133 e-ISSN 2477-6416
URL : https://jurnal.uns.ac.id/ijap/article/view/81259
Indonesian Journal of Applied Physics (IJAP) Vol. 14 No. 2 page 234
DOI : https://doi.org/10.13057/ijap.v14i2.82159

FABRICATION OF CERIUM OXIDE-GRAPHENE OXIDE NANOCOMPOSITE USING ULTRASOUND-ASSISTED PRECIPITATION METHOD

Iis Nurhasanah*[1], Arvia[1], Nor Basid Adiwibawa Prasetya [2], Ahmad Jauhari[1]
[1]Department of Physics, Faculty of Science and Mathematics, Diponegoro University, Indonesia
[2]Department of Chemistry, Faculty of Science and Mathematics, Diponegoro University, Indonesia
*nurhasanah@fisika.fsm.undip.ac.id

Received 05-12-2023, Revised 14-09-2024, Accepted 18-10-2024,
Available Online 18-10-2024, Published Regularly October 2024

ABSTRACT

The cerium oxide-graphene oxide nanocomposite was fabricated by ultrasound-assisted precipitation method and characterized using Fourier transform infrared, UV-Vis spectroscopy, X-ray diffractometer, and transmission electron microscope. The Fourier transform infrared spectra displayed the O-H, C=C, and C-H vibrations indicating the interaction between cerium oxide and graphene oxide. The broad absorption of around 300 nm is ascribed to the superposition of cerium oxide and graphene oxide absorption peaks. X-ray diffraction pattern analysis suggests the creation of graphene oxide nanosheets with an interlayer spacing of 0.821 nm. The transmission electron microscope image showed that the cerium oxide nanoparticles dispersed on the graphene oxide nanosheet. These findings exhibit the useful ultrasound-assisted precipitation method for fabricating cerium oxide-graphene oxide nanocomposite.

Keywords: cerium oxide; graphene oxide; nanocomposite; ultrasound

Cite this as: Nurhasanah, I., Arvia., Prasetya, N. B. A., & Jauhari, A. 2024. Fabrication of Cerium Oxide-Graphene Oxide Nanocomposite Using Ultrasound-Assisted Precipitation Method. *IJAP: Indonesian Journal of Applied Physics, 14*(2), 234-242. doi: https://doi.org/10.13057/ijap.v14i2.81259

INTRODUCTION

Nanotechnologies and nanomaterials are now applied in various industries due to their attributes, like a large surface-to-volume ratio, size effects, catalytic capability, and reactivity. Nanomaterials-based cerium oxide (CeO_2) has additional valuable characteristics, including low cost, non-toxicity, strong chemical stability, and high electron transfer capacity. These qualities are the result of the dual oxidation states coexisting in the CeO2 nanomaterials. In particular, the CeO_2 nanoparticles are considered promising multifunctional nanomaterials. The reversible valence characteristic and distinct crystal structure of CeO_2 nanoparticles facilitate the creation of oxygen vacancies, resulting in a structure rich in defects. These properties determine performance applications of CeO_2 nanoparticles such as catalysts in energy conversion[1], supercapacitors [2], anti-corrosion [3], adsorbents [4], and biomedical applications [5-6]. Another intriguing material for creating nanoscale structures is graphene oxide (GO), which has exceptional electrical conductivity, a huge specific surface area, and oxygenated groups. The distinctive of GO properties is the potential for numerous applications[2],[7-10].

Nevertheless, using separate CeO_2 nanoparticles and GO nanosheets exhibits limited performance in different applications. For instance, GO tends to form an aggregate that reduces its surface area [2],[9],[11]. This phenomenon is affected by the interlayer spacing of GO. In contrast, CeO_2 has poor dispersion as filler in the polymer matrix. Therefore, to overcome these problems, CeO_2 and GO are functionalized and mixed to generate the synergetic effect of CeO_2-GO hybrid or nanocomposites. To construct specific features for development and sustainable applications, the CeO_2-GO nanocomposite has been synthesized through different synthesis techniques, such as hydrothermal [10],[12], ultrasonicated-mixture of GO and CeO_2 [13],[14], a sonochemical method [15,16] and facile chemical co-precipitation method[2]. The synthesis technique affected the formation of CeO_2-GO nanocomposite [17],[18]. Thus far, the hydrothermal approach is the most useful and applicable technique for creating CeO_2-GO composites due to a single step decorating the GO network [11]. In contrast to the ultrasonication of mixed GO and CeO_2, which prepares the CeO_2-GO composite through multiple stages. However, there is a limitation in the cost of hydrothermal equipment. On the other hand, precipitation is regarded as an efficient and cost-effective method for synthesizing CeO_2-GO composite due to simple preparation and apparatus [2], nonetheless, it requires calcination at moderate to high temperatures.

This study describes the fabrication of CeO_2-GO nanocomposite utilizing an ultrasound-assisted precipitation approach, which differs from the synthesis method used in previous studies. Cavitation by ultrasound generates hot spots in the surrounding atmosphere, leading to the composite formation at low temperatures and with short calcination times. GO nanosheets were synthesized through graphite oxidation usage a modified Hummer's method. Numerous characterization techniques consisting of Fourier transform infrared, UV-visible spectroscopy, X-ray diffraction, and transmission electron microscope were applied to analyze the structure, optical properties, and morphology of CeO_2-GO nanocomposite. As a comparison, the CeO_2 was also synthesized and characterized.

METHOD

Synthesis of GO nanosheets

GO was synthesized using a modified Hummer's method [19]. The synthesis begins by dissolving 1 g of graphite in 46 ml of H_2SO_4 at a temperature of 0 -5^oC for 2 hours. The graphite solution was then treated with 0.5 g of $NaNO_3$ and 6 g of $KMnO_4$ and agitated for two hours. The stirring operation was continued for 24 hours at 35^oC. Then 100 ml of distilled water was poured into the solution. After 1 hour, 5 ml of 30% H_2O_2 was added and agitated for 1 hour to eliminate the residual $KMnO_4$. The solution mixture was centrifuged at 3000 rpm for 20 minutes, separating the supernatant and filtrate. The filtrate was neutralized with 5% HCl and distilled water before drying at 80^oC for 12 hours to produce black powder. The powder was mixed with distilled water and ultrasonically proceeded for 90 minutes. The powder was then separated with a centrifuge at 3000 rpm for 20 minutes. To get dry powder, the heating phase was carried out for 12 hours at 80^oC.

Fabrication of CeO_2-GO nanocomposite

A composite of CeO_2-GO was synthesized using the procedure adopted from the literature with slight modification, especially in the ultrasonication and heating process [20]. This process was created by dissolving one gram of $Ce(NO_3)_3.6H_2O$ and dispersing GO in 100 mL demineralized water separately. The appropriate amount of GO was weighted to obtain a mass ratio of GO to cerium nitrate of 3%. After stirring the GO suspension for an hour, the $Ce(NO_3)_3$ solution was gradually added. Next, the 5% HCl solution was dropped until it reached pH 3, followed by adding 30 wt.% H_2O_2 solution. Then the precipitant of 0.5 wt.% NaOH was poured into the solution up to its pH of 10. After 30 minutes of ultrasonic wave radiation, the solution was left for 24 hours. Distilled water was used to wash the precipitate until the pH reached neutrality. Subsequently, it was heated at $80^{O}C$ for 6 hours to obtain dry powder. CeO_2 was synthesized using the procedure described in previously reported [21].

Characterization

The Fourier Transform Infrared (FTIR, Perkin Elmer) spectrum was employed to identify a functional group, which verified the creation of the CeO_2-GO composite. The absorbance spectrum of the CeO_2-GO composite was measured using the UV-Vis spectrophotometer (Shimadzu). The X-ray diffraction pattern of the CeO_2-GO composite was recorded using an X-ray diffractometer (Miniflex Rigaku) equipped with a Cu K_α radiation source with a wavelength of 1.5406 Å. To ascertain the CeO_2-GO composite's structural parameter, the x-ray diffraction data was examined using the Bragg diffraction law, and the Scherrer formula described in Eq (1) and Eq (2) respectively.

$$d_{(hkl)} \sin\theta = \lambda \tag{1}$$

$$L = \frac{k\lambda}{\beta \cos\theta} \tag{2}$$

In this case, d denotes a spacing layer, L stands for crystallite size, θ is the diffraction angle, λ wavelength, and β full width at half maximum (FWHM). The *h*, *k*, and *l* are Miller indices. Furthermore, the CeO_2-GO composite's nanostructure morphology was examined using a transmission electron microscope (TEM, Talos F200X) with an accelerating voltage of 120 kV. To demonstrate the successful synthesis of the CeO_2-GO composite, the same characterization was also carried out on GO and CeO_2.

RESULTS AND DISCUSSION

GO, CeO_2, and CeO_2-GO have been successfully synthesized. The products were in powder form. Figure 1 shows the photograph of GO, CeO_2, and CeO_2-GO powder. The GO powder is dark black which is similar to other researchers [22],[23] and commercial GO [24]. The CeO_2 powder is light yellow which is similar to our previous research [4,21], while the CeO_2-GO powder is dark grey. The dark grey color indicates the formation of the CeO_2-GO composite. GO powder was made through a modified Hummer's method from graphite oxidation with a heating process at a temperature of $80^{o}C$. CeO_2 powder and CeO_2-GO composite were synthesized using an ultrasound-assisted precipitation method that was continued with a heating process at a temperature of $80^{o}C$. Figure 2 depicts the schematic diagram of GO and GO-CeO_2 formation.

(a) GO (b) CeO_2 (c) CeO_2 - GO

Figure 1. Photograph of powder for (a) GO, (b) CeO_2, and (c) CeO_2-GO composite

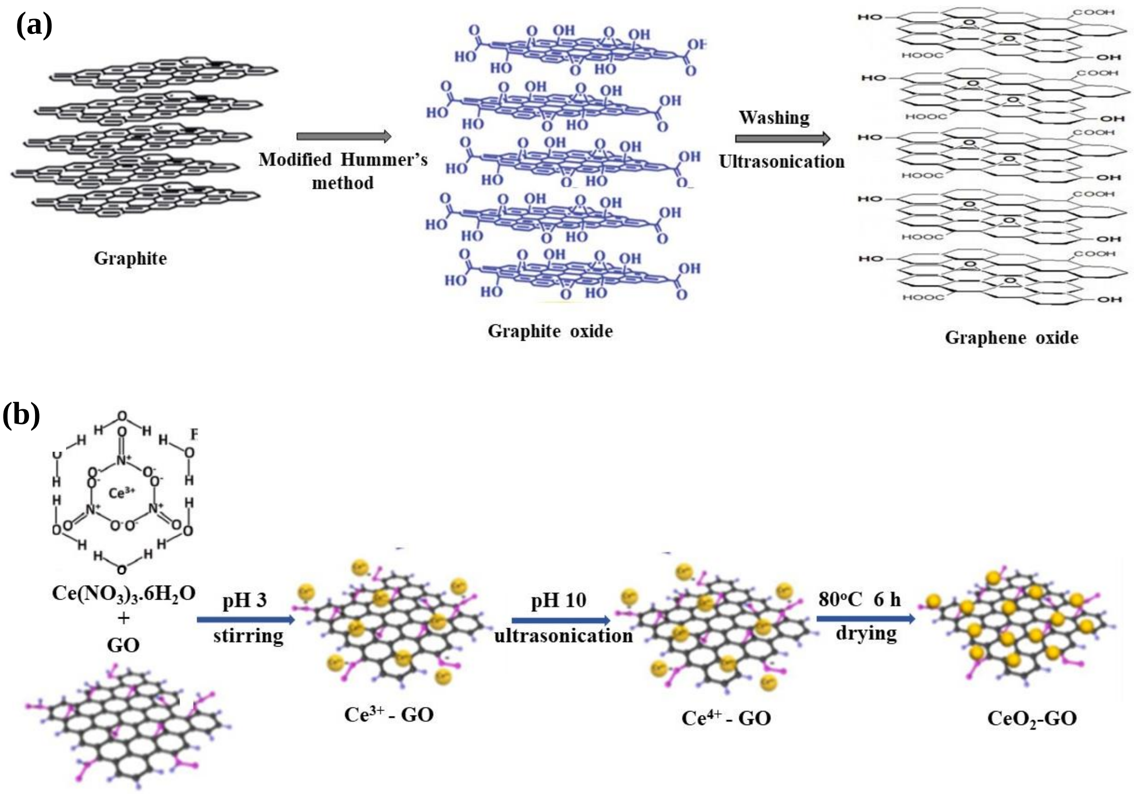

Figure 2. Schematic illustration of formation (a) GO and (b) CeO_2-GO

The formation of the CeO_2-GO composite was clarified by the functional group analysis FTIR spectrum as depicted in Figure 3. The O-H stretching vibration of the acid is represented by an absorption band at wave number 3422 cm^{-1} in the FTIR spectra of GO, while a prominent peak with a C=C stretching vibration is seen at 1633 cm^{-1}. The C-O vibration was shown by another peak in the FTIR spectra of GO, located at 1078 cm^{-1} [25]. Five absorption bands displaying O-Ce-O vibrations at 475 cm-1, O-C-O stretching vibrations at 1384 cm^{-1}, and C=C stretching vibrations at the same wave number as GO are visible in the FTIR spectra of CeO_2 [21],[26]. Overall, it can be seen that GO, CeO_2 and CeO_2-GO have the same spectra for C=C stretching vibrations, O-H stretching, and C-H bending vibrations [27]. The CeO_2-GO composite has been properly synthesized because the interaction between GO and CeO_2 during the composite's synthesis did not produce any additional bonds.

Further analysis of the formation of CeO_2-GO was obtained from the UV-Vis absorption spectrum. Figure 4(a) displays the GO absorption spectra. The absorption peak is located in the UV region, at 231 nm and 307 nm. The covalent link between the carbon atoms that created the hexagonal arrays is responsible for the absorption peak at 231 nm, which is typical of the π-π*plasmon of the C=C aromatic bond. While the n-π* transition of the C=O carbonyl group is represented by the absorption peak at 307 nm. The result is consistent with other research [23],[28],[29]. UV-Vis absorption spectrum analysis indicates the existence of functional groups with oxygen that attach to carbon on the surface of GO. The UV-Vis absorption spectrum of the CeO_2-GO composite as displayed in Figure 4(c) revealed broad absorption at 250 to 380 nm as a result of the absorption peak overlapping of the CeO_2 with the GO peak. This analysis also confirmed the CeO_2-GO composite formation. A similar spectrum was investigated on CeO_2-GO composite prepared by microwave heating [30].

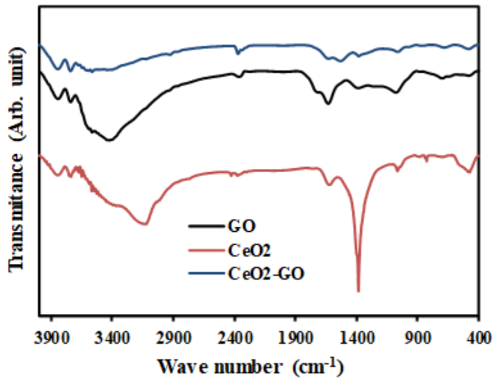

Figure 3. FTIR spectra of GO, CeO_2 nanoparticles, and CeO_2-GO nanocomposite

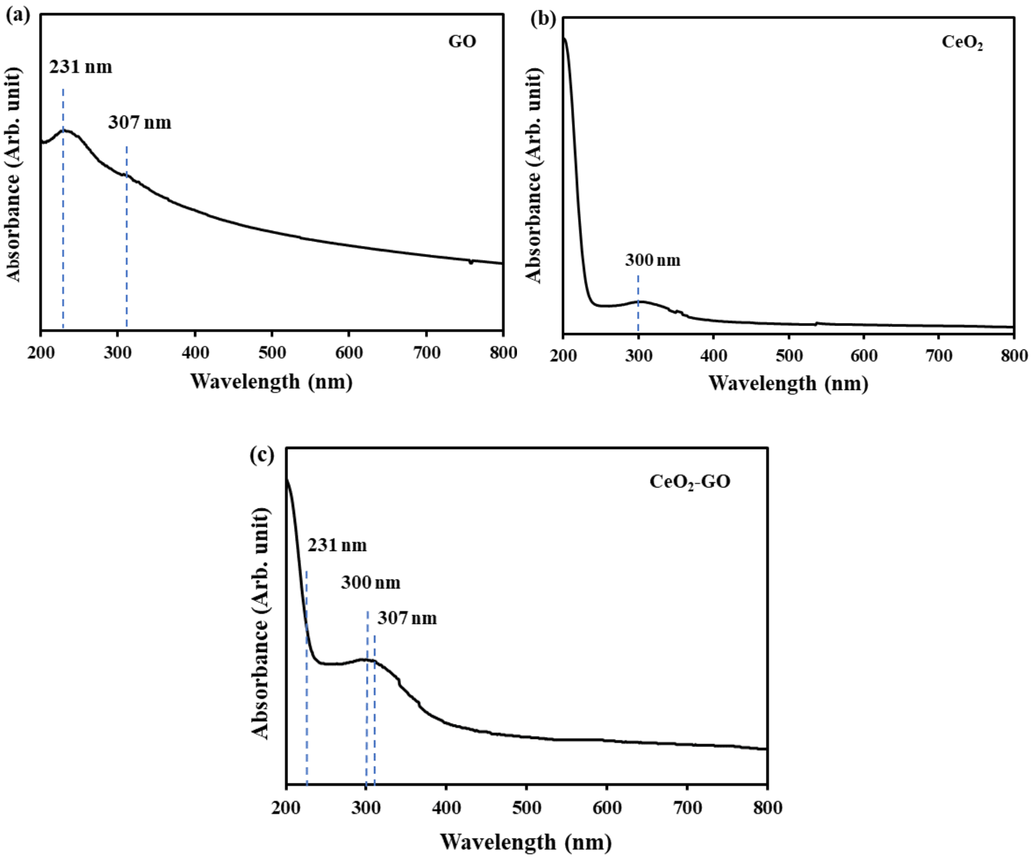

Figure 4. UV-Vis spectra of GO, CeO_2 nanoparticles, and CeO_2-GO nanocomposite

The X-ray diffraction patterns of GO, CeO_2, and CeO_2-GO were recorded at 2θ of 5 to 85^o to verify the nanostructure formation of the CeO_2-GO composite. GO, CeO_2 and CeO_2-GO composite X-ray diffraction patterns are depicted in Figure 5(a). A diffraction peak at 2θ = 10.76^o appeared in the X-ray diffraction pattern of GO. A diffraction peak with low intensity was also observed at 2θ = 42.79^o. Referring to JCPDS-ICDD No. 82-2261, the diffraction peaks correspond to the (002) and the (100) plane reflection of GO, respectively [22,26,31]. The X-ray diffraction pattern of GO in this study is in agreement with commercial GO [24], and other studies [32]. Thus, GO has been successfully synthesized employing a modified

Hummer's method for the oxidation of graphite. Equation (1) was utilized to calculate an interlayer spacing ($d_{(002)}$) of 0.821 nm, which is associated with a 2-theta of 10.76^o. This interlayer spacing is more than the typical 0.335 nm interlayer spacing of graphite [12,33,34]. This finding reveals that different oxygen functional groups are formed in the carbon surface layer, which reduces the van der Waals attraction force among graphene layers [9]. At the same time, the appearance of the 2θ of 42.79^o indicates distortion in the stacked graphene layers. The Scherrer formula in Equations (2) was used to calculate the average height L_c and the average diameter L_a of stacking layers by inserting k values of 0.89 and 1.84, respectively. Moreover, these parameters of GO structures can be seen in the schematic illustration in Figure 5(b). Then in the X-ray diffraction pattern of CeO_2, diffraction peaks were observed at 2θ = 28.53^o; 33.06^o; 47.13^o; 56^o; 69.46^o; and 76.85^o which represents the crystallographic planes of the (111), (200), (220), (311), (400), and (331). These diffraction peaks are by JCPDS-ICDD No. 34-0394 for the cubic structure of CeO_2 [4,21,26,35]. The calculated crystallite size of CeO_2 nanoparticles was 7,3 nm using the Scherrer formula for (111) diffraction peak.

Meanwhile, CeO_2-GO only shows CeO_2 diffraction peaks with lower intensity and wider FWHM than the pristine CeO_2 diffraction peaks. The diffraction peaks of GO were not observed, possibly due to the following reasons: the higher crystallinity of CeO_2 than GO, the incorporation of CeO_2 in GO distorts the GO structure and the concentration of GO in the composite is relatively small. A similar characteristic was also observed in previous research[2,10,13]. In addition, it can be observed that a shift in several X-ray diffraction peak positions of CeO_2 in CeO_2-GO towards the smaller 2θ of pure CeO_2. The shifting in the 2θ angle of the peak position shows the formation of a new material of CeO_2-GO composite which has different characteristics from their constituent materials. Thus, it can be said that the synthesis method is effective in creating the CeO_2-GO composite. Meanwhile, the wide FWHM for CeO_2-GO indicates the formation of a composite with a very tiny crystallite size. By applying the Scherrer formula in Equation (1), the average crystallite size of the CeO_2-GO nanocomposite was 1.6 nm. The crystallite size of the composite is smaller than the crystallite size of the constituent. The obtained research data shows the effectiveness of CeO_2-GO nanocomposite synthesis.

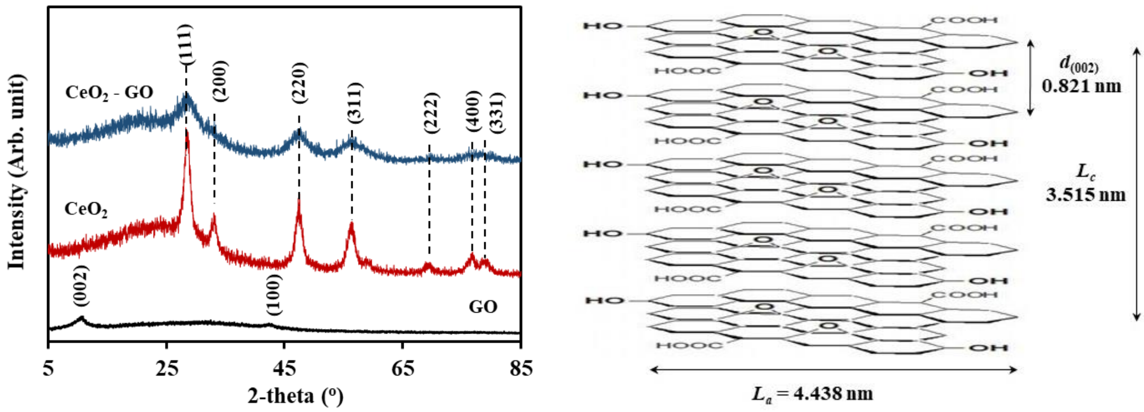

Figure 5. (a) X-ray diffraction patterns of GO, CeO_2, and CeO_2-GO, (b) schematic illustration of the GO structure

An electron transmission microscope (TEM) was used to examine the morphology of GO, CeO_2, and CeO_2-GO. The GO nanosheets can be seen in Figure 6(a). The formation of GO nanosheets is regarded as a combination of oxygen structures containing functional groups of C-O, C=O, and O-H on the surface of the graphene layer as confirmed by FTIR spectrum analysis [36]. Figure 6(b) shows spherical particles with a size of around 10 nm for CeO_2 and Figure 5(c) shows CeO_2 particles with a very tiny size dispersed on GO nanosheet. In contrast to other CeO_2 nanoparticles and CeO_2-GO nanocomposites prepared by the hydrothermal method, showed agglomerated spherical shape particles [10],[30]. Only some CeO_2 particles appear to stick together in this study, this could be the result of tiny particles growing together during the cerium reduction process. The TEM image reveals the presence of an active site on the GO sheet for the deposition of CeO_2 nanoparticles configuration of CeO_2-GO nanocomposite.

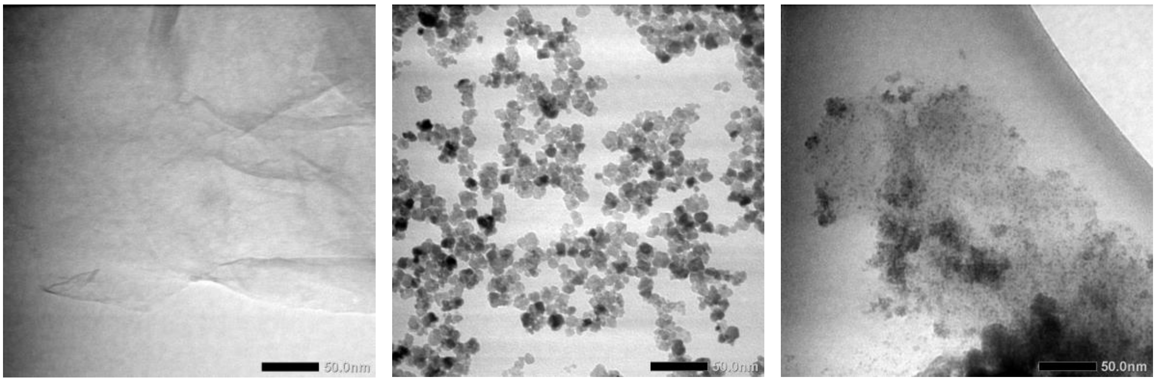

(a) (b) (c)

Figure 6. TEM image of (a) GO sheet, (b) CeO_2 nanoparticles and (c) GO- CeO_2 nanocomposite

CONCLUSION

The ultrasound-assisted precipitation route was used for the fabrication of CeO_2-GO composites. FTIR spectrum analysis indicated that the CeO_2-GO composite contains a functional group of the constituent composite, there are C=C, O-H stretching vibrations, and C-H bending vibrations. The CeO_2-GO composite formation was validated by the broad UV spectrum with an absorption peak at about 300 nm. The nanostructure of CeO_2-GO composite with a crystallite size of 1.61 nm was confirmed from XRD and TEM analysis. The CeO_2-GO composite has the potential as an anticorrosive and antibacterial coating in medical applications.

REFERENCES

1 Li, Q., Song, L., Liang, Z., Sun, M., Wu, T., Huang, B., Luo, F., Du, Y., & Yan, C.H. 2021. A Review on CeO_2 -Based Electrocatalyst and Photocatalyst in Energy Conversion. *Adv. Energy Sustainability Res*. 2021, 2, 2000063

2 Deng, D., Chen, N., Xiao, X., Du, S., & Wang, Y. 2017. Electrochemical performance of CeO_2 nanoparticle-decorated graphene oxide as an electrode material for supercapacitor. Ionics, 23, 121-129.

3 Valero-Gomez, A., Molina, J., Pradas, S., López-Tendero, M. J., & Bosch, F. 2020. Microencapsulation of cerium and its application in sol–gel coatings for the corrosion protection of aluminum alloy AA2024. Journal of Sol-Gel Science and Technology 93(1)

4 Nurhasanah, I., Kadarisman, Gunawan, G., Sutanto, H. 2020. Cerium oxide nanoparticles application for rapid adsorptive removal of tetracycline in water. *J. Environ. Chem. Eng*., 8, 103613.

5 Pansabal. S., Oza, R., Borgave, S., Chauhan, A., Bardapurkat, P., Vyas, S. & Ghotekar, S. 2022. Bioengineered cerium oxide (CeO2) nanoparticles and their diverse applications: a review. *Appl. Nanosci.*, 13(5), 6067-6092.

6 Shcherbakov, A.B., Reukov, V.V., Yakimansky, A.V., Krasnopeeva, E.L., Ivanova, O.S., Popov, A.L., & Ivanov, V.K. 2021. CeO_2 Nanoparticle-Containing Polymers for Biomedical Applications: A Review. Polymers, 13(6), 924.

7 Sontakke, A.D., Tiwari, S., & Purkait, M.K. 2023. A comprehensive review on graphene oxide-based nanocarriers: Synthesis, functionalization, and biomedical applications. *Flat. Chem*., 38, 100484.

8 Panda, P.K., Dash, P., Yang, J.M., &Chang, Y.H. 2022. Development of chitosan, graphene oxide, and cerium oxide composite blended films: structural, physical, and functional properties. *Cellulose*, 29, 2399–2411.

9 Yu, W., Sisi, L., Haiyan, Y., & Jie, L. 2020. Progress in the functional modification of graphene/graphene oxide: a review. *RSC Adv*., 10, 15328.

10 Channei, D., Nakaruk, A., & Phanichphant, S. 2017. Influence of graphene oxide on photocatalytic enhancement of cerium dioxide. *Mater. Let*., 209, 43-47.

11 Nemati, F., Rezaie, M., Tabesh, H., Eid, K., Xu, G., Ganjali, M.R., Hosseini, M., Karaman, C., Erk, N., Show, P.L., are, N., & Karimi-Maleh, H. 2022. Cerium functionalized graphene nanostructures and their applications; A review. *Environ*. *Res*., 208, 112685.

12 Zhongguan, H., Qiang, Z., Sen, L., Zhang, G., Nadeem, A., & Ge, Y. 2023. Cost-effective one-spot hydrothermal synthesis of graphene oxide nanoparticles for wastewater remediation: AI-enhanced approach for transition metal oxides. *Chemosphere*, 337, 139064.

13 Iqbal, A., Ahmad, T., Qais, F.A., Ahmad, N., Shafi, A., Ahmed, A.S., & Srivastava, S. 2023. Proficient visible-light-driven photocatalytic and anti-biofilm activity of biosynthesized CeO_2-graphene oxide nanocomposites. *Mater*. *Chem*. *Phys*., 298, 127397.

14 Saranya, J., Sreeja, B.S., Padmalaya, G., Radha, S., & Manikandan, T. 2020. Ultrasonic Assisted Cerium Oxide/Graphene Oxide Hybrid: Preparation, Anti-proliferative, Apoptotic Induction and G2/M Cell Cycle Arrest in HeLa Cell Lines. *J. Inorg*. *Organomet*. *Polym*. *Mater*., 30, 2666–2676.

15 Muthukrishnaraj, A., Kalaivani, S.S.,, Mankandan, A., Kavitha, H.P., Srinivasan, R., & Balasubramanian, N. 2020. Sonochemical synthesis and visible light-induced photocatalytic property of reduced graphene oxide@ZnO hexagonal hollow rod nanocomposite. *J. Alloys Compd*., 836, 155377

16 Esmaeili, C, Norouzi, P., Zar, M.S., Eskandari, M., Faridbod, F., & Ganjaliet, M.R. 2019. A FFT square wave voltammetry sensing method for highly sensitive detection of phytic acid using a cerium oxide nanoparticles decorated graphene oxide. *J. Electrochem*. *Soc*. 166 (15), B1630–B1636.

17 An, H., Liu, L., Song, N., Zhu, H., & Tang, Y. 2021. Rational design and synthesis of cerium dioxide-based nanocomposites. *Nano Res*., 16(3), 3622-3640.

18 Mishra, S.R., & Ahmaruzzaman, Md. 2021. Cerium oxide and its nanocomposites: Structure, synthesis, and wastewater treatment applications. *Mater*. *Today Commun*., 28, 102562.

19 Prasetya, N.B.A., Ajizan, A.I., Widodo, D.S., Ngadiwiyana, & Gunawan. A polyeugenol/graphene composite with excellent anti-corrosion coating properties. *Mater*. *Adv*., 2023,4, 248

20 Ma, L., Wang, X., Wang, J., Zhang, J., Y., C., Fan, L., & Zhang, D. 2021. Graphene oxide–cerium oxide hybrids for enhancement of mechanical properties and corrosion resistance of epoxy coatings. *J. Mater*. *Sci*., 56, 10108–10123.

21 Paramita, S.A., Nurhasanah, I., & Khumaeni, A. 2023. Structural and Optical Properties of Bismuth-doped Cerium Oxide Prepared at a Low Temperature. *JPFA*, 13(01), 16-24.

22 Hulagabi, M.M., Vesmawala, G.R., & Patil Y.D. 2023. Synthesis, characterization, and application of graphene oxide and reduced graphene oxide and its influence on rheology, microstructure, and mechanical strength of cement paste. *J. Build. Eng*., 71, 106586.

23 Stobinski, L., Lesiak, B., Malolepszy, A., Mazurkiewicz, M., Mierzwa, B., Zemek, J., Jiricek, P., & Bieloshapka, I. 2014. Graphene oxide and reduced graphene oxide studied by the XRD, TEM and electron spectroscopy methods. *J. Electron. Spectros. Relat. Phenomena,* 195, 145–154.

24 Yuwen, C., Liu, B., Zhou, B., Tian, S., & Zhang, L. 2021. Structure and properties of graphene oxide during the synthesis process at fixed temperatures. *Ceram. Int*., 47, 17487–17493.

25 Zankana, M.M., Al-dalawy, S.M., & Barzinjy, A.A. 2023. Synthesis and characterization of bio-nanocomposites: Functionalization of graphene oxide with a biocompatible amino acid. *Hybrid Adv*. 3, 100070.

26 Huang, K., Li, Y.H., Lin, S., Liang, C., Xu, X., Zhou, Y.F., Fan, D.Y., Yang, H.J., Lang, P.L., Zhang, R., Wang, Y.G., & Lei, M. 2014. One-step synthesis of reduced graphene oxide–CeO_2 nanocubes composites with enhanced photocatalytic activity. *Mater. Let.*, 124, 223–226.

27 Ojha, G.P., Pant, B., Park, S.J., Park, M., Kim, H.Y. 2017. Synthesis and characterization of reduced graphene oxide decorated with CeO_2-doped MnO_2 nanorods for supercapacitor applications. *J. Colloid Interface Sci*., 494, 338–344.

28 Amrollahi, S., Ramezanzadeh, B., Yari, H., Ramezanzadeh, M., & Mahdayian, M., 2019. In-situ growth of ceria nanoparticles on graphene oxide nanoplatelets to be used as a multifunctional (UV shield/radical scavenger/anticorrosive) hybrid compound for exterior coatings. *Prog. Org. Coat*., 136, 105241.

29 Ciplak, Z., Yildiz, N, & Calimli, A. 2014. Investigation of Graphene/Ag Nanocomposites Synthesis Parameters for Two Different Synthesis Methods. *Fuller. Nanotub. Carbon Nanostructure*, 23, 361–370.

30 Anand, K., Murugan, V., Roopan, S.M., Surendra, T.V., Chuturgoon, A.A., & Muniyasamy, S. 2018. Degradation Treatment of 4-Nitrophenol by *Moringa oleifera* Synthesised GO-CeO_2 Nanoparticles as Catalyst. *J. Inorg. Organomet. Polym. Mater*., 28, 2241–2248.

31 Panigrahi, M., & Avar, B. 2022. Synthesis and Characterization of Binary Reduced Graphene Oxide/Metal Oxide Nanocomposites. *Phys. Chem. Solid State*, 23(1), 101-112.

32 Emiru, T.F., & Ayele, D.W. Controlled synthesis, characterization and reduction of graphene oxide: A convenient method for large scale production. *Egypt. J. Basic Appl. Sci*., 4, 74-79.

33 Cakmak, G., & Ozturk, T. 2019. Continuous synthesis of graphite with tunable interlayer distance. *Diam. Relat. Mater.*, 96, 134-139.

34 Li, C., Lu, Y., Yan, J., Yu, W., Zhao, R., Du, S., & Niu, K. 2021. Effect of long-term aging on graphene oxide: structure and thermal decomposition. *R. Soc. Open Sci*. 8: 202309.

35 Jayakumar, G., Irudayaraj, A.A., Raj, A.D. 2017. Particle Size Effect on the Properties of Cerium Oxide (CeO_2) Nanoparticles Synthesized by Hydrothermal Method. *Mater. Sci. Eng.*, 9(1): 1-5.

36 Alam, S.N., Sharma, N., & Kumar, L. 2017. Synthesis of Graphene Oxide (GO) by Modified Hummers Method and Its Thermal Reduction to Obtain Reduced Graphene Oxide (rGO). *Graphene,* 6, 1-18.